PNAS RESEARCH ARTICLE | ENGINEERING OPEN ACCESS

Miniaturized metachronal magnetic artificial cilia

Zhiwei Cui[a,b], Ye Wang[a,b], Shuaizhong Zhang[c], Tongsheng Wang[a,b], and Jaap M. J. den Toonder[a,b,1]

Edited by Joanna Aizenberg, Harvard University, Cambridge, MA; received March 22, 2023; accepted July 14, 2023

Biological cilia, hairlike organelles on cell surfaces, often exhibit collective wavelike motion known as metachrony, which helps generating fluid flow. Inspired by nature, researchers have developed artificial cilia as microfluidic actuators, exploring several methods to mimic the metachrony. However, reported methods are difficult to miniaturize because they require either control of individual cilia properties or the generation of a complex external magnetic field. We introduce a concept that generates metachronal motion of magnetic artificial cilia (MAC), even though the MAC are all identical, and the applied external magnetic field is uniform. This is achieved by integrating a paramagnetic substructure in the substrate underneath the MAC. Uniquely, we can create both symplectic and antiplectic metachrony by changing the relative positions of MAC and substructure. We demonstrate the flow generation of the two metachronal motions in both high and low Reynolds number conditions. Our research marks a significant milestone by breaking the size limitation barrier in metachronal artificial cilia. This achievement not only showcases the potential of nature-inspired engineering but also opens up a host of exciting opportunities for designing and optimizing microsystems with enhanced fluid manipulation capabilities.

metachronal motion | miniaturization | magnetic artificial cilia (MAC) | flow generation

Significance

We created both symplectic and antiplectic miniaturized metachronal motion of arrays of identical magnetic artificial cilia by integrating a paramagnetic substructure in the substrate underneath the cilia and applying a simple uniform magnetic field. This method enables us to create wave-like motion of arrays of miniaturized artificial cilia, mimicking the metachronal motion of biological cilia, breaking the size limitation of existing methods, and making it possible to integrate them in small-scale microfluidic chips. Both types of metachronal motion generated flow at both high and low Reynolds numbers. Our results prove that the metachrony plays an important role in flow generation and that the effect depends on the metachronal wave propagation direction.

Cilia, microscopic hair-like external cell organelles, are ubiquitously present in nature (1–7). They cover the outer surfaces of microorganisms such as Paramecia, and they also appear in the human body (8–11), for example, on the inner surfaces of the trachea and the lungs, where they exhibit an asymmetric whip-like oscillatory motion with an effective and a recovery stroke (8, 9, 12, 13). Moreover, neighboring cilia move slightly out of phase which results in collective metachronal motion. There are three types of metachronal motion, determined by the wave propagation direction: symplectic, antiplectic, and laeoplectic motion, where the wave propagates in the same, opposite, and perpendicular direction to the cilia effective stroke (1–3, 6, 14–16). In this way, cilia generate flow resulting in the swimming of microorganisms or the transport of mucus in the airways (11). This is quite effective, for example, the active cilia on Parameciae are able to propel these microorganisms at a speed of 10 times their own body length per second (3, 17). Researchers have been developing artificial cilia to mimic the flow generation by biological cilia for application in microfluidic devices (18). Magnetic artificial cilia (MAC) are the most prominent, and they have a number of advantages over other artificial cilia classes like pneumatically driven artificial cilia (4), light-driven artificial cilia (19, 20), and electrostatically-driven artificial cilia (21): The actuation by an external magnetic field does not require any complex external physical connections, and the magnetic field does not interfere with biological process within the microfluidic chip.

Many biological cilia show metachronal motion, and since this benefits flow generation, it has been widely studied also for artificial cilia recently both numerically (1, 2, 6, 22–30) and experimentally (3, 8, 12, 16, 31–33). Numerical simulations have confirmed that metachronal motion can enhance flow generation compared with synchronous motion (2, 9, 24, 28). Several experimental studies have presented MAC that were designed and fabricated to mimic and study metachronal motion (3, 7–9, 12, 31–33). In these studies, two different methods have been used to realize the metachronal motion of MAC, both of which are difficult to miniaturize. In the first method, a complex external magnetic field is applied to create different magnetic forces on neighboring identical cilia (3, 8, 34). In our earlier approach, we, for example, used an actuation setup consisting of an array of rod-shaped millimeter-sized permanent magnets mounted on a belt that was translated underneath the microfluidic device containing a MAC array. This generated a time-dependent nonuniform but periodic magnetic field, resulting in a phase difference between the responses of the identical consecutive MAC, and thus metachrony (3, 34). The second method has been realized by tuning the magnetic anisotropy of the individual MAC in an array, in particular by aligning the magnetic particles within the MAC to different angles between consecutive cilia, or by varying

Author affiliations: [a]Department of Mechanical Engineering, Eindhoven University of Technology, Eindhoven 5600 MB, The Netherlands; [b]Institute for Complex Molecular Systems, Eindhoven University of Technology, Eindhoven 5600 MB, The Netherlands; and [c]Max Planck Institute for Intelligent Systems, Stuttgart 70569, Germany

Author contributions: Z.C., Y.W., S.Z., and J.M.J.d.T. designed research; Z.C. performed research; Z.C. analyzed data; Y.W. reviewed and edited the manuscript; S.Z. realized the actuation setup realization, reviewed and edited the manuscript; T.W. established the simulation model; J.M.J.d.T. reviewed and edited the manuscript; and Z.C., T.W., and J.M.J.d.T. wrote the paper.

The authors declare no competing interest.

This article is a PNAS Direct Submission.

[1]To whom correspondence may be addressed. Email: J.M.J.d.Toonder@tue.nl.

This article contains supporting information online at https://www.pnas.org/lookup/suppl/doi:10.1073/pnas.2304519120/-/DCSupplemental.

Published August 23, 2023.

the length of the cilia within an array, and actuating the cilia array by a rotating uniform magnetic field (8, 12, 16, 31–33, 35). However, both these approaches have been demonstrated for relatively large artificial cilia (hundreds of micrometers long) only, and they are hard to be miniaturized which limits implementation in microfluidic devices such as for point-of-care or organ-on-chip applications. The first method faces limitations primarily due to the size constraints imposed by the actuation magnets. The second method encounters difficulties in spatially controlling magnetic particle alignment for closely spaced MAC; this challenge becomes particularly pronounced when attempting to achieve high precision alignment required for miniature cilia. Furthermore, it should be noted that existing methods can only achieve either symplectic or antiplectic metachronal motion using the same patch of cilia, limiting the versatility of the motion patterns that can be achieved. These limitations highlight the need for further advancements in the development of techniques that can overcome these size constraints of metachronal artificial cilia. Addressing these challenges would greatly enhance the capabilities and applicability of magnetically actuated cilia systems.

In this paper, we introduce a method that allows for miniaturization of MAC at least down to dozens of micrometers long, does not require a complex external field to be applied, works with arrays of identical cilia, and enables both symplectic and antiplectic metachrony. The key idea is to create a paramagnetic substructure within the substrate underneath the array of identical MAC and apply a simple external rotating uniform magnetic field. The paramagnetic substructure is magnetized by the external magnetic field and perturbs the external field to generate a time-dependent local magnetic field. When well dimensioned, neighboring identical cilia will experience a different magnetic field at any instant and metachrony will occur even if the external magnetic field is uniform and the MAC are identical. Using this approach, we achieved metachronal motion of MAC with different sizes, and we could achieve metachronal wave propagation in different directions by simply changing the relative position of the substructure with respect to the MAC array, analogous to symplectic and antiplectic metachrony. In this paper, we also confirm and further analyze the actuation mechanism using numerical simulations, and we quantitatively assess the flow generation of the two metachronal motions under both high and low Reynolds number conditions.

In this study, we realize metachronal motion of small MAC which can be miniaturized even further, e.g., toward artificial cilia with biological dimensions (36, 37), breaking the size limitation of earlier approaches, with the possibility to realize two types of metachronal motion. It is also possible to adjust the wavelength of metachrony by design of the geometry of the magnetic substructure. Our findings represent a crucial advancement toward the seamless integration of MAC into microfluidic chips at a small scale.

Results

Actuation and Metachronal Motion of MAC. We fabricated the MAC using micromolding from a mixture of Ecoflex 00-30 and paramagnetic carbonyl iron powder (CIP). The fabrication process is shown in Fig. 1*A*; the experimental methods section provides a detailed description. Two different sizes of cylinder-shaped MAC were fabricated: larger MAC with a diameter of 50 μm and a length of 300 μm and smaller MAC with a diameter of 25 μm and a length of 150 μm. The fabrication procedures of both MAC were identical, but the mold for the larger MAC was made using photolithography of SU-8 photoresist, and that of the smaller MAC with femtosecond laser machining of fused silica, as indicated in Fig. 1*A*. The resulting larger and smaller MAC are shown in Fig. 1 *B*, *ii* and *iii*, respectively. Note that we fixed the aspect ratio of both the larger and the smaller cilia to six, because of the fabrication limitation posed by photolithography, since the UV illumination will be nonuniform if we enlarge the ratio of the MAC, leading to ill-defined MAC shapes. Identically for all MAC, the magnetic CIP particles were linearly aligned along the MAC length during fabrication. To realize metachronal motion, therefore, the magnetic field consecutive MAC experience should be different. To realize this while still applying a uniform rotational external magnetic field to actuate the cilia array, we integrated a rod-shaped paramagnetic substructure with a diameter of 4.5 mm underneath the cilia array as sketched in Fig. 1 *B*, *i*. The fabrication process of the magnetic substructure is shown in Fig. 1*C*; details of the process are described in the experimental section. The resulting magnetic substructure and the MAC are shown in Fig. 1 *B*, *iv*. The distance between the bottom of the MAC and the top of the magnetic substructure, which is determined by the thickness of the pure PDMS layer in between, is around 100 μm. The actuation setup that generates a rotational uniform magnetic field is shown in Fig. 1 *D*, *i*. To observe the motion of the MAC, we made the holder shown in Fig. 1 *D*, *ii*, which was positioned in the setup at the center of the magnetic field. To characterize the induced fluid flow, we made a second holder shown in Fig. 1 *D*, *iii*. The details of the PDMS channel are shown in *SI Appendix*, Fig. S1.

A patch with a row of six MAC was attached on top of the paramagnetic substructure, a side view of which is shown in Fig. 1 *B*, *iv*. The integrated MAC and substructure were mounted in the holder designed for MAC observation, shown in Fig. 1 *D*, *ii*. Fig. 2 *A* and *B* show the resulting metachronal motion of the larger MAC (diameter 50 μm, length 300 μm, and pitch 450 μm), obtained from experiments and finite element simulations, respectively, when applying a uniform counterclockwise rotating field with a magnitude of 150 mT and a rotation frequency of 5 Hz.

The resulting MAC motion in water is shown in Fig. 2*A* in side view. Each individual MAC exhibits 2D reciprocal motion while neighboring cilia show a phase difference, indeed resulting in metachronal motion, which we call "metachrony No. 1" for reasons that will become clear later. The tip displacement of all six MAC as a function of time, as obtained from an analysis of the experiment, is shown in Fig. 2*C*. The curves are numbered corresponding to the MAC numbering in Fig. 2*A*. Initially, the individual MAC follow the rotating motion of the external magnetic field due to the magnetic torque they experience, bending to the left; this phase is called magnetic stroke. As the MAC bend during this stroke, they accumulate elastic energy, determined by the mechanical properties of the MAC. Once the cilia tip location reaches a critical leftmost position, the magnetic torque diminishes, and the associated magnetic energy cannot balance the accumulated elastic energy anymore. As a consequence, the cilia will start to move upward and whip back elastically to the right at high speed, releasing their elastic energy. This phase is called the elastic stroke. This stroke ends beyond the initial position (0 μm), after which the cilia are picked up by the magnetic torque again and start bending to the left. Note, that the MAC beating frequency (10 Hz) equals twice the actuation frequency of the external magnetic field (5 Hz). The most important observation from Fig. 2*A* is that indeed the motion of the MAC is phase shifted in time, with No. 1 starting the elastic stroke at 0.046 s, followed by the whipping back of No. 2 to No. 6 cilia (at 0.061 s) in their number sequence order. The wave direction is to the left, opposite to the direction of the elastic stroke. The corresponding experimental video is available in the Movie S1. It is important to acknowledge that the

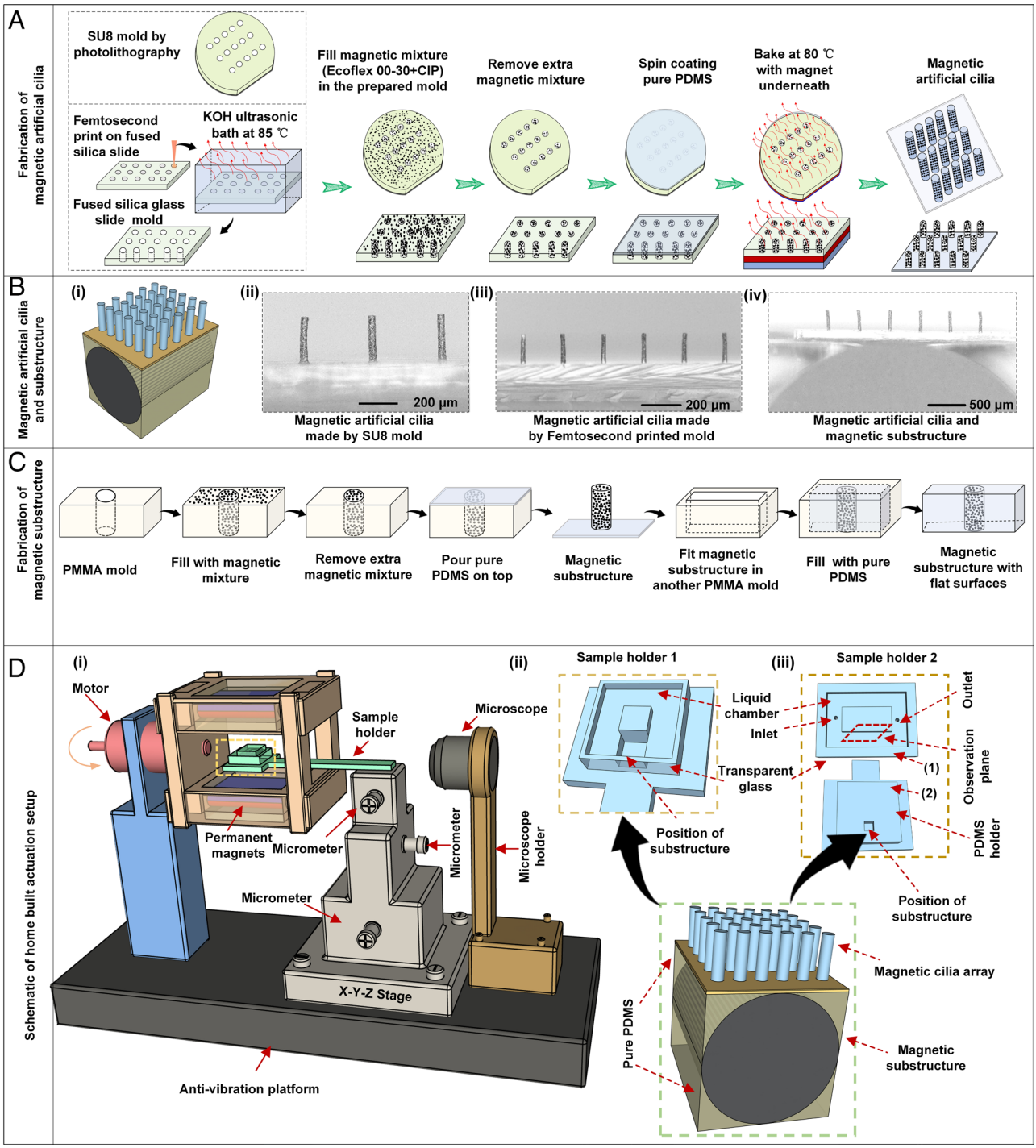

Fig. 1. Fabrication process of magnetic artificial cilia (MAC), paramagnetic substructure, and homebuilt actuation setup. (*A*) Schematic of the fabrication process of the MAC. We used two methods to fabricate the mold: For larger MAC with a diameter of 50 μm, we used photolithography, and for miniaturized cilia with a diameter of 25 μm, we applied femtosecond laser machining to make the mold. The following steps are the same. (*B*, *i*) Schematic of the integrated MAC and magnetic substructure. (*ii*) Side view of a row of the MAC with a diameter of 50 μm. (*iii*) Side view of the miniaturized MAC with a diameter of 25 μm. (*iv*) Side view of the integrated MAC and magnetic substructure. (*C*) Fabrication process of the magnetic substructure. (*D*, *i*) Schematic of the homebuilt magnetic actuation setup which can induce a uniform magnetic field of ~150 mT at the center of the working space. (*ii*) Schematic of the 3D-printed holder allowing for observing the motion of MAC. (*iii*) Schematic of the closed PDMS holder for observing the generated fluid flow, details are available in *SI Appendix*, Fig. S1.

intricate motion of the cilia is not only influenced by the magnetic actuation but also by the shape and mechanical properties of the MAC. The geometry and flexibility of the MAC can significantly impact the overall performance and functionality of the cilia system. Although the potential influence of these factors is recognized, it is crucial to emphasize that the primary focus of the current study lies on investigating the method to realize the miniaturization of metachronal motion of MAC arrays. Consequently, conducting a detailed exploration of the specific impact of MAC shape and mechanical properties falls outside the scope of this research endeavor. However, it is worthwhile to pursue such investigation in future research.

We carried out finite element simulations using COMSOL to understand and predict the MAC motion. The details of the

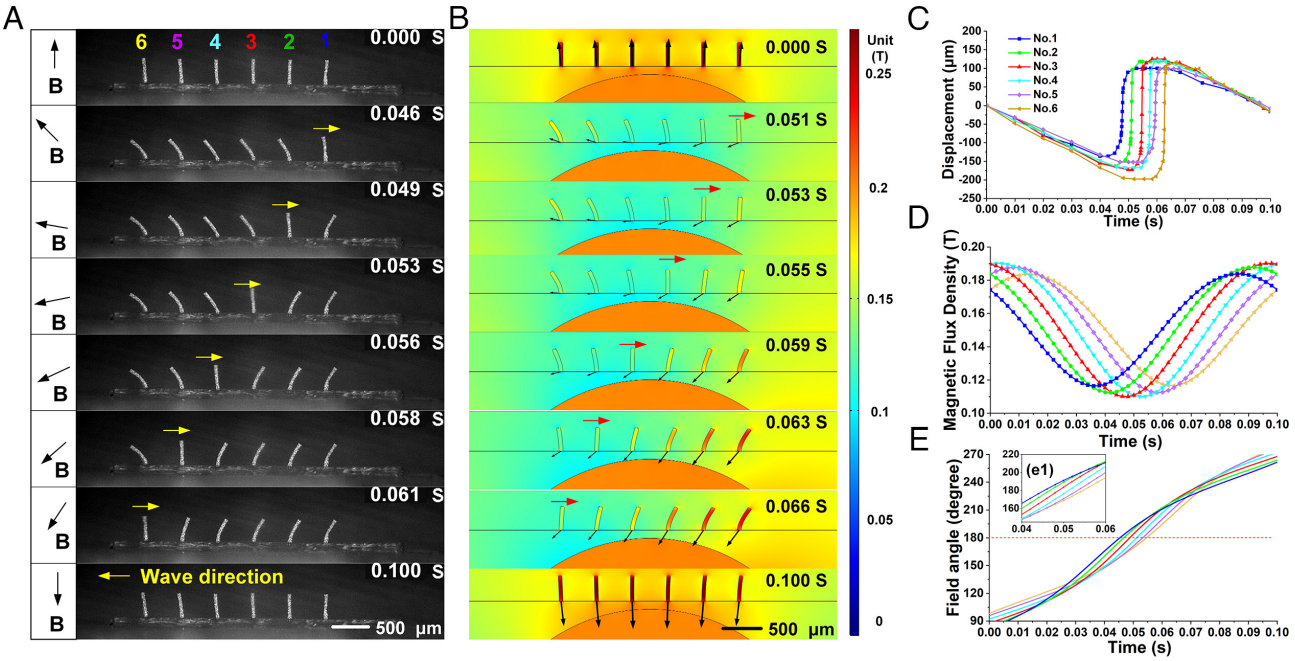

Fig. 2. Metachronal motion of magnetic artificial cilia with a diameter of 50 μm, "metachrony No. 1"; results both from experiment and simulation. (*A*) Experimental results: side view of the metachronal MAC motion resulting from the presence of the integrated magnetic substructure, actuated with a uniform field of 150 mT rotating counterclockwise at 5 Hz. Note: the MAC beating frequency equals twice the actuation frequency of the external magnetic field. The video is available as Movie S1. (*B*) Corresponding simulation results obtained using finite element simulations with COMSOL. The color bar indicates the magnitude of the magnetic field (flux density). The external magnetic field applied is 150 mT. The local magnetic field above the magnetic substructure becomes time-dependent and is periodic with the rotation of the external magnetic field. The black arrows at the MAC positions indicate the local magnetic field direction and the length of the arrow is proportional to the magnitude of the local magnetic field. The corresponding video can be found in Movie S2. (*C*) Tip displacement of the MAC based on the experimental results obtained by ImageJ software analysis. The number sequence in the figure corresponds with the numbers indicated in *A*. The tip location in the upright MAC position is taken as 0 μm. Locations to the left of this initial position are defined as negative, to the right as positive. (*D*) Local magnetic field (magnetic flux) magnitude as a function of time at the position of each cilium, obtained from the simulation results. (*E*) Angle of the local magnetic field as a function of time at the position of each cilium, obtained from the simulation results; (*e1*) zooms in to the figure when the magnetic field direction crosses 180°.

COMSOL model can be found in the *SI Appendix* document. The results are shown in Fig. 2*B*, and they are in good agreement with the experimental results of Fig. 2*A*—the motion of the individual MAC and the metachronal behavior are very similar, even though the exact timing of the MAC motion differs somewhat, probably attributable to slight experimental variations in the experimental MAC. The similarity can also be appreciated from the corresponding simulation results video, in Movie S2. The colors in the figure indicate the magnetic field magnitude (flux density). The black arrows at the MAC locations indicate the local magnetic field direction, and their length is proportional to the field magnitude. The simulation results clearly show that the local magnetic field surrounding the paramagnetic substructure is nonuniform since the substructure locally perturbs the applied uniform field. Due to the rotation of the applied field, the local field is time-dependent and periodic. Fig. 2 *D* and *E* show the details of the simulated magnetic field at the MAC locations. The curves in Fig. 2*D* represent the magnitude of local magnetic field (flux density) at the position of each cilium, in which the colors agree with the number sequence color indicated in Fig. 2 *A* and *C*. The external uniform magnetic field strength applied in the model is 150 mT. Due to the presence of the paramagnetic substructure, the local magnetic field strength is different between MAC at any time, and it is time-dependent and periodic due to the rotation of the applied field. For all cilia, the maximum magnetic flux density in one period is around 190 mT and the minimal value is around 120 mT, but the minimum is reached at different time points, first for No. 1 and then in the order of MAC number sequence. Fig. 2*E*, depicting the magnetic field orientation for all MAC during one beating cycle, shows a similar trend. The initial MAC orientation is around 90°, followed by a 180° rotation during one cycle, which corresponds to half a rotation of the applied field. The orientation around 180° is critical since this is approximately the moment at which the elastic stroke of the MAC starts. The zoomed-in figure (Fig. 2 *E*, *e1*) clearly shows that the sequence of the local magnetic field when they cross 180° position is according to the MAC number sequence order. Taken together, from the simulation results, we conclude that the metachronal motion of the MAC is caused by the phase shift of the local magnetic field, both in amplitude and in direction, between the MAC locations, by the presence of the magnetic substructure.

In addition to the case shown in Fig. 2, we realized the metachronal motion of 8 MAC and 10 MAC with the same dimension. In these cases, we kept the magnetic substructure the same, but changed the pitch between neighboring cilia to fit to the substructure size, which means the metachronal wavelength is the same. The resulting motion is shown in *SI Appendix*, Figs. S2 and S3, and the corresponding movies are available in Movies S3 and S4.

Miniaturization of Metachronal Motion. Miniaturization of metachronal motion is crucial for applying MAC in microfluidic devices. One of the significant advantages of our method is that it allows for this miniaturization. To demonstrate the feasibility of this method, we made a batch of smaller MAC, with a cilia diameter of 25 μm, a cilia length of 150 μm, and a pitch between cilia of 225 μm; we intentionally kept the aspect ratio equal to that of the larger cilia for good comparison. The diameter of the paramagnetic substructure was kept at 4.5 mm, implying that the wavelength of the metachronal motion will remain the same as

for the larger MAC. We used 11 miniaturized MAC in one array and integrated this with the paramagnetic substructure. Again, we applied a rotating magnetic field (150 mT, 5 Hz) to actuate the MAC. The experimental results are shown in Fig. 3*A*, and the corresponding video is available in Movie S5. Fully equivalent to the larger MAC, the smaller MAC also exhibit metachronal motion. In addition, the MAC tip displacement determined from the experiment is shown in Fig. 3*C*, in which the MAC numbers agree with those in Fig. 3*A*. Similar to the larger MAC, each of the miniaturized magnetic cilia shows a whip-like motion, with an initial magnetic stroke bending to the left following the magnetic field direction, up to a threshold at the leftmost position

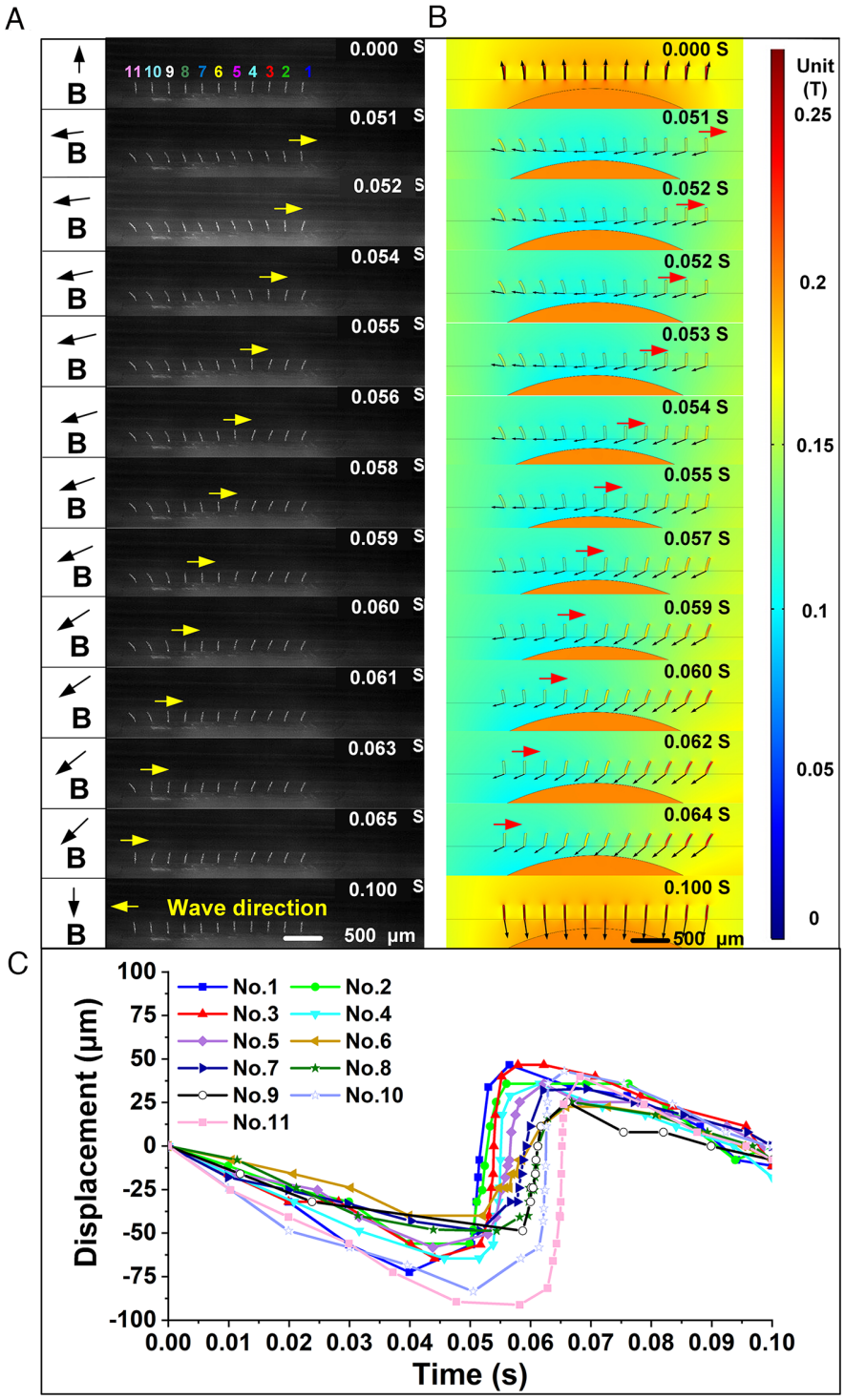

Fig. 3. Metachronal motion of miniaturized MAC (diameter 25 μm). (*A*) Experimental result: side view of the metachronal miniaturized MAC motion resulting from the presence of the integrated magnetic substructure, actuated with a uniform field of 150 mT rotating counterclockwise at 5 Hz. Note: the MAC beating frequency equals twice the actuation frequency of the external magnetic field. The video is available as Movie S5. (*B*) Corresponding simulation results obtained using finite element simulations with COMSOL. The color bar indicates the magnitude of the magnetic field (flux density). The external magnetic field applied is 150 mT. The black arrows at the MAC positions indicate the local magnetic field direction, and the length of the arrow is proportional to the magnitude of the local magnetic field. (*C*) Tip displacement of the miniaturized MAC based on the experimental results of (*A*). The tip location in the upright MAC position is taken as 0 μm. Locations to the left of this initial position are defined as negative, to the right as positive.

after which the cilia exhibit a fast elastic stroke to the right. The rightmost tip position is around 50 μm, exceeding to the initial position, 0 μm. Then, the MAC start the magnetic stroke again bending leftward. The curves for the individual MAC shown in Fig. 3*C* are shifted in time, with No. 1 exhibiting the elastic stroke first, after which the other MAC follow in the sequence of MAC number. Fig. 3 *A* and *C* show that the metachronal wave travels to the left, opposite to the elastic stroke direction.

We also carried out finite element simulations of the miniaturized MAC using COMSOL, with all parameters equal to those used in the experiment. The simulation results are shown in Fig. 3*B*, where the colors indicate the magnitude of the magnetic field. The simulated MAC array indeed shows metachronal motion which is in good agreement with the experimental results of Fig. 3*A*. The simulation results clearly show that this is due to the nonuniform, time-dependent, and periodic magnetic field that is induced by the magnetic substructure perturbing the applied uniform rotating field.

This demonstrates that miniaturized metachronal motion can be realized by our method. In the future, the MAC can be miniaturized further even down to biological cilia sizes to truly mimic ciliary motion in nature (36, 37). The wavelength of the metachronal motion can be changed by changing the diameter or the geometry of the substructure.

Reversing the Wave Direction of the Metachronal Motion of Artificial Cilia. In nature, cilia can exhibit different types of metachrony: symplectic metachrony in which the wave travels in the direction of the effective stroke of individual cilia and antiplectic metachrony in which the wave travels opposite to the effective stroke. However, achieving diverse forms of metachronal motion in MAC presents challenges due to the inherent difficulty in inducing directional reversals of the metachronal wave, which typically leads to corresponding reversals in the motion of individual MAC. Consequently, the resulting overall motion is merely mirrored, while the fundamental metachronal nature remains unaltered. But with our method, we are able to reverse the metachronal wave direction while keeping the nature of the individual cilia motion the same. This can be achieved by changing the relative position between MAC and paramagnetic substructure, as shown in *SI Appendix*, Fig. S4. In the cases shown in Figs. 2 and 3, the magnetic substructure is positioned symmetrically underneath the MAC array (we call this metachrony No. 1). Now, we shift the magnetic substructure to the left relative to the MAC array, keeping all other parameters the same (we call this metachrony No. 2). The resulting MAC motion in experiments is shown in Fig. 4*A*, in which the external magnetic field rotates counterclockwise, like in the cases we presented earlier. The corresponding video is available in Movie S6. Indeed, we see a reversal of the metachronal wave compared to Fig. 2. From Fig. 4*C*, showing the experimentally obtained tip displacement as a function of time for all MAC, it is clear that the individual MAC still exhibit the same reciprocal motion as in Fig. 2, with a magnetic stroke to the left and a fast elastic stroke to the right. However, the order in which the MAC start with the elastic stroke is different: Cilium No. 6 goes first, after which the other MAC follow in reverse sequence of MAC number. Note that the MAC with the numbers 6, 5, 4, and 3 start their elastic stroke with a very short time difference but still in a reversed number order. Hence, we have realized a metachronal wave traveling to the right, in the same direction as the elastic stroke.

We carried out finite element simulations using COMSOL to understand and predict the MAC motion in this metachrony No. 2 condition, the results of which are shown in Fig. 4*B*. The shift

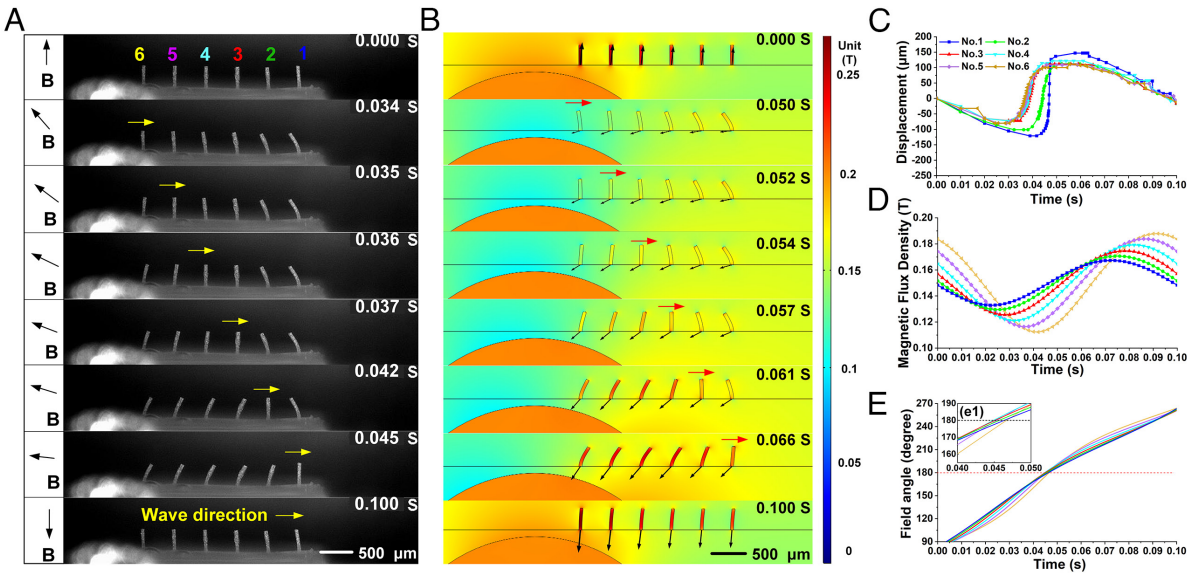

Fig. 4. Reversing the wave direction of the metachronal motion of magnetic artificial cilia with a diameter of 50 μm by shifting the relative position between MAC and magnetic substructure, "metachrony No. 2", shown by both experiments and simulations. (*A*) Experimental result: side view of the metachronal MAC motion resulting from the presence of the integrated magnetic substructure, actuated with a uniform field of 150 mT rotating counterclockwise at 5 Hz. The wave direction is reversed compared to Figs. 2 and 3. The corresponding video is available as Movie S6. (*B*) Corresponding simulation results obtained using finite element simulations with COMSOL. The color bar indicates the magnitude of the magnetic field (flux density). The external magnetic field applied is 150 mT. The local magnetic field above the magnetic substructure becomes time-dependent and is periodical with the rotation of the external magnetic field. The black arrows at the MAC positions indicate the local magnetic field direction, and the length of the arrow is proportional to the magnitude of the local magnetic field. Note that the position of the magnetic substructure is different from that in Figs. 2 and 3, and this causes the wave direction reversal. (*C*) Tip displacement of the MAC based on the experimental results. The number sequence in the figure corresponds with the numbers indicated in *A*. The tip location in the upright MAC position is taken as 0 μm. Locations to the left of this initial position are defined as negative, to the right as positive. (*D*) Local magnetic field magnitude as a function of time at the position of each cilium, obtained from the simulation results of (*B*). (*E*) Orientation angle of the local magnetic field as a function of time at each MAC location, obtained from the simulation results. (*e1*) Zoom in to the figure when the magnetic field direction crosses 180°.

of the location of the magnetic substructure can be clearly seen here (compare with Fig. 2*B*). The results agree well with the experimental findings, confirming the reversal of the metachronal wave direction for this arrangement, although the timings of the individual MAC motion are somewhat different, likely due to variation in experimental MAC properties. The corresponding simulation video can be found in Movie S7. Fig. 4 *D* and *E*, respectively, show the simulated magnitude and angle of the local magnetic field at the position of each cilium as a function of time. A comparison of these results (metachrony No. 2) with Fig. 2 *D* and *E* (metachrony No. 1) reveals similarities and differences. For both metachronies, the field magnitude at each MAC location initially decreases, reaches a minimum, and then rises up to maximum, and the curves of the different MAC are time shifted in the same way with No. 1 reaching the minimum first and No. 6 reaching it last. However, while the field magnitudes for different MACs in metachrony No. 1 (Fig. 2*D*) display a comparable range, the field magnitudes for metachrony No. 2 (Fig. 4*D*) exhibit notable differences. In particular, the initial value for MAC No. 6 is substantially larger than for MAC No. 1, but it drops much faster to a lower minimal value. This discrepancy arises due to variations in the distances between MACs and the magnetic substructure. In terms of the magnetic field angle curves, the distinctions observed in metachrony No. 2 (Fig. 4*E*) are relatively minor when compared to those observed in metachrony No. 1 (Fig. 2*E*), particularly around the 180° mark.

It is clear from the simulations that the existence of the paramagnetic substructure induces a local magnetic field that is nonuniform, time dependent, and periodic. The initiation of the elastic stroke in the MAC is determined by the delicate interplay between the magnetic torque, influenced by the field magnitude and angle, and the accumulated elastic torque, influenced by the degree of MAC bending and hence by the MAC's stiffness. For metachrony No. 2, our analysis shows that this is governed by a delicate combination of local field magnitude and direction: If the local field has dropped sufficiently and the field angle has proceeded enough, the magnetic artificial cilium starts its elastic stroke. In metachrony No. 2, this results in a reversed metachronal wave compared to metachrony No. 1.

Flow Generation by Metachronal Motion. The generation of fluid flow is a vital application of MAC. For flow induced by biological cilia, metachrony can play an essential role, for example, for the propulsion of microorganisms and for transportation of mucus in the airways. Fluid flow generation by biological cilia is achieved by two mechanisms. First, the reciprocal motion of individual cilia is usually asymmetric, i.e., it consists of an effective stroke and a recovery stroke. In the effective stroke, the cilium maximizes its effect on the fluid by moving in a straight and upright way, whereas in the recovery stroke, the cilium minimizes its effect on the fluid by moving in a bent shape and/or close to the surface. This asymmetric motion can be quantified by the so-called total swept area, which is defined as the area enclosed by the traces of the cilia tip during the effective and recovery stroke; this is zero when both traces are identical and nonzero if they are different. Flow generation is in the direction of the effective stroke when the swept area is nonzero. Second, metachrony plays a role, but how is not fully understood yet. The consensus now is that antiplectic metachrony enhances the flow that is generated by asymmetric cilia motion, and symplectic metachrony reduces it; a possible mechanism for this is the shielding of flow between neighboring cilia (2, 24). For biological cilia, the speed of cilia motion and cilia sizes are relatively small so that biological cilia operate at low Reynolds number (smaller than 1), i.e., subject to Stokes flow conditions, and therefore, inertial effects do not play a role in fluid flow generation. The Reynolds number is the ratio of the fluid inertia to the fluid drag force, which we define here as $\mathrm{Re} = \rho\nu L/\mu$, where Re is the Reynolds number, ρ is the density of the fluid, ν is the flow speed, L is the length of the MAC, and μ is the dynamic viscosity of the fluid. With this definition, Re represents the local condition at the cilia tips. For low Re, a difference in speed between forward and backward strokes does not lead to net fluid transport. In certain artificial cilia conditions, however, large cilia speeds may be generated which lead to a possible third flow generation mechanism for artificial cilia, next to the other two mentioned. Namely, for sufficiently high Reynolds numbers, inertia may not be neglected if the cilia motion has a fast and a slow stroke, flow may be generated in the fast stroke direction. In this section, we analyze the flow generation by the different metachronal motions created by our approach, as discussed above, in which we will consider the contribution of these different mechanisms.

To be able to observe the flow generation, we made a closed transparent PDMS rectangular channel as shown in Fig. 1 *D*, *iii* and *SI Appendix*, Fig. S1, including a transparent glass surface on the observation side. Details of the fabrication of the channel can be found in the experimental section. The paramagnetic substructure was mounted at the position indicated in Fig. 1 *D*, *iii*. A patch of MAC array consisting of $6 \times 5 = 30$ cilia was attached on top of the substructure. The PDMS channel has a width of 3 mm and a height of 500 μm. The microfluidic device was mounted in the center of the rotational magnetic field, and the magnetic field was rotated in the counterclockwise direction as depicted in Fig. 5 *A*, *i*. As shown above, the MAC array then shows metachronal motion, in which the wave direction will be different for the two studied cases metachrony No. 1 and No. 2, as indicated in Fig. 5 *A*, *ii*. Each cilium in the array shows a 2D whip-like motion, with a slower magnetic stroke to the left and a faster elastic stroke to the right, as shown in Fig. 5 *A*, *iii*. The angle between the two extreme positions of the MAC is defined as "the opening angle", indicated as α in Fig. 5 *A*, *iii*. In addition to the metachrony cases, we carried out experiments in which the magnetic substructure was omitted from the microfluidic chamber, so that the MAC beat almost synchronously but still with the characteristic magnetic and elastic strokes; in one of these configurations, we applied a counterclockwise rotating magnetic field just like for the metachrony cases, and in the other, we used a clockwise rotation. We used both water and glycerol in the experiments; since the latter has a viscosity that is about 1,000 times larger than that of the former, inertial effects in glycerol flow will be absent because of low Reynolds number conditions, whereas they may be present in water. The fluid flow speed was measured at the geometrical center of the microfluidic channel. Fig. 5 *A*, *iv* defines the positive flow direction as that in which the fluid travels in the direction of the magnetic stroke (for counterclockwise magnetic field rotation).

The flow generation results are shown in Fig. 5 *B* and *C*. For the water flow generation (Fig. 5*B*), the following phenomena are observed, which we will list here first and discuss in more detail later. First, in all cases, the water flow velocity increases in magnitude with frequency, and it is generated in the direction of the elastic stroke, suggesting that inertia plays an important role. Second, for the no metachrony cases, the water flow direction changes from negative to positive when the magnetic field rotation is changed from counterclockwise to clockwise, but the values are not perfectly symmetric around zero. This is probably due to manufacturing imperfections. Third, compared with the control group (no metachrony, counterclockwise actuation), the metachrony No.

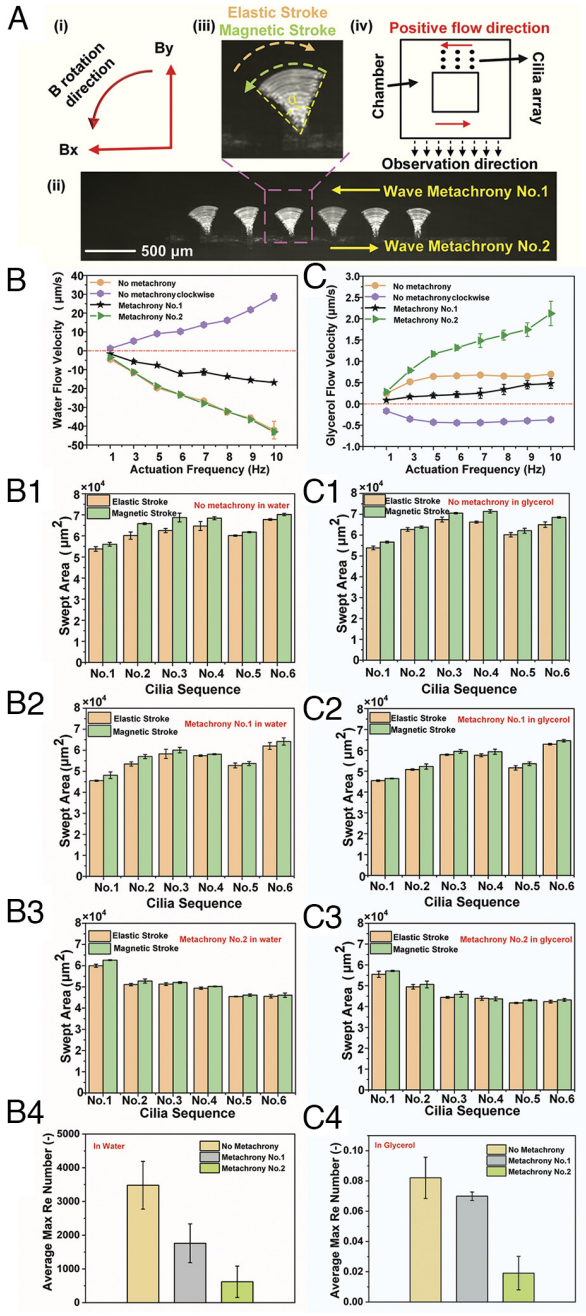

Fig. 5. Flow generation of metachronal MAC motions in both high and low Reynolds number conditions. (*A, i*) Schematic of the default counterclockwise rotation direction of the applied external magnetic field. (*ii*) Superposed time-lapse images of MAC motion generated by the integrated magnetic substructure, indicating the metachronal wave propagation direction of metachrony No. 1 and No. 2. (*iii*) Side view of one cilium (composed of superposed images taken in one actuation period), where the α represents the opening angle of the cilium. The green dash line indicates the direction of the magnetic stroke, and the orange dash line indicates the direction of the elastic stroke when the cilium is actuated with an external magnetic field rotating counterclockwise. (*iv*) Schematic of top view of the flow channel. The MAC array is put on one side of the channel, and the fluid flow observation location is opposite to the cilia position. The red arrow indicates the positive flow direction, which is in the magnetic stroke direction of the MAC when actuated with a counterclockwise rotating field. (*B*) Water flow generation by the two metachronal motions and two control groups without metachrony. (*C*) Glycerol flow generation by the two metachronal motions and two no-metachrony control groups. (*B1–B3*) Swept areas by MAC during the magnetic stoke and elastic stroke in water for the two metachronal motions and the control group (counterclockwise field rotation). (*C1–C3*) Swept areas by MAC during the magnetic stoke and elastic stroke in glycerol for the two metachronal motions and the control group (counterclockwise field rotation). (*B4* and *C4*) Calculated local maximal Reynolds number in water and glycerol at 10 Hz based on the maximum tip speed in *SI Appendix*, Fig. S5. Data shown in all panels are calculated by at least three independent experiments. Error bars indicate the SD.

1 group shows decreased flow generation of water; the metachrony No. 2 group, on the other hand, generates almost equal water flow velocities as the control group. The maximal water flow velocity, at 10 Hz actuation (in which the magnetic field rotates at 5 Hz), generated by the control group is around 42 μm/s. The metachrony No. 1 group generates a flow rate of 17 μm/s, while it is 43 μm/s for the metachrony No. 2 group.

To better understand the contributions of the three mechanisms mentioned above to the net flow generation: asymmetry, metachrony, and inertia, we now analyze in more detail the swept area which is related to the effect of asymmetry. According to Fig. 5 *B1–B3*, the swept areas of the magnetic stroke for the three cases (no metachrony, and metachrony No. 1 and No. 2) are all slightly larger than those of the elastic stroke, which means the flow generated by the asymmetric motion will be in the magnetic stroke direction. However, as shown in Fig. 5*B*, the flow generation is in the negative direction for all cases, i.e., the direction of elastic stroke. For the no metachrony group, the metachrony mechanism is absent, and thus, we can conclude from that case that the water flow generation by inertia dominates over the effect of asymmetry. Indeed, a quantitative analysis of the cilia tip speed (*SI Appendix*, Fig. S5) shows that the maximal Reynolds number is much larger than one during the elastic stroke when the MAC are actuated at 10 Hz, which is shown in Fig. 5*B4*. From this figure, the Reynolds number is the largest for the no metachrony group, followed by the metachrony No. 1 and then the metachrony No. 2 group, suggesting that the flow generation by inertia also should be different, with decreasing flow in the same sequence. Clearly, from Fig. 5*B*, this is not the case. The metachrony No. 2 group even generates equal flow as the no metachrony group, even though it is expected to be much less based on the weaker inertial effect. The explanation for this observation is that the metachronal wave (for metachrony No. 2 traveling in the direction of the elastic stroke and hence in the direction of the generated flow) in fact adds to generate flow that compensates for the loss of inertial contribution. The flow generation of the metachrony No. 1 group is smallest (Fig. 5*B*), even though its inertial contribution is suggested to be in between the two other cases as shown in Fig. 5*B4*. From this, we can conclude that the metachronal contribution of the metachrony No. 1 group, in which the wave propagation direction is opposite to the elastic stroke and hence counter to the flow generation direction, is lower than the metachrony No. 2 group where the wave direction is reversed. Taken together, the metachrony indeed has a substantial influence on the generated fluid flow, and the effect depends on the metachronal wave propagation direction.

From the results for the glycerol flow generation (Fig. 5*C*), we can make several main observations. First, in all cases, the glycerol flow is generated in the direction of the magnetic stroke, i.e., positive for counterclockwise magnetic field rotation and negative for clockwise magnetic field rotation; the magnitude of the velocity initially increases with actuation frequency, but levels off for higher frequencies. Second, for the no metachrony cases, the glycerol flow direction changes from positive to negative when the magnetic field rotation is changed from counterclockwise to clockwise, but the values are not perfectly symmetric around zero. This is probably due to manufacturing imperfections. Third, the metachrony No. 1 motion induces lower flow velocity than the control group (no metachrony), while the metachrony No. 2 motion substantially enhances the flow velocity. The maximal glycerol flow velocity, at 10 Hz actuation (in which the magnetic field rotates at 5 Hz), generated by the control group is around 0.7 μm/s, while it decreases to 0.5 μm/s for the metachrony No. 1 group and increases to 2.1 μm/s for the metachronyal No. 2 group.

The viscosity of glycerol is 1,000 times larger than that of water, and this reduces the MAC tip speed largely due to viscous drag (*SI Appendix*, Fig. S5). This results in low Reynolds number conditions, Re <<1 (see Fig. 5*C4*), which means that inertial effects will not play a role in contrast to the water experiments, but the combination of the asymmetric and metachronal motion will determine the glycerol flow generation. As can be seen in Fig. 5 *C1–C3*, for all the three cases, the swept area of the magnetic stroke is larger than the elastic stroke. In this case, we can make the analogy with biological cilia, and call the magnetic stroke the "effective" stroke, and we expect the asymmetric motion to generate a flow in the effective/magnetic stroke direction, which is indeed what we observe. The metachrony also has an effect on flow generation. For metachrony No. 1, the metachronal wave propagation is in the same direction as the effective/magnetic stroke, analogous to symplectic metachrony, and the flow generation is diminished compared to the no metachrony group. For metachrony No. 2, the metachronal wave propagation is opposite to the effective/magnetic stroke, analogous to antiplectic metachrony, and the flow generation is enhanced compared to the no metachrony group. This is in agreement with previous findings from numerical simulations (2, 6, 9, 22, 24, 28).

The generated flow velocities in glycerol are much lower than in water. Clearly, the inertial effects that are present in water are quite effective in inducing fluid flow. In glycerol, the motion of the MAC is much influenced by the viscosity of the liquid. The leveling off of the flow velocity with actuation frequency (Fig. 5*C*) is a consequence of this: The motion of the cilia is reduced by increased viscous drag, as is clear from measurements of the MAC opening angle (*SI Appendix*, Fig. S6), and this results in a decrease of the generated flow in glycerol.

Finally, we should note that the no metachrony control group should theoretically show perfectly synchronous motion. However, due to slight differences in properties due to material and processing imperfections, this was not the case, and the sequence of MAC response is somewhat random, see *SI Appendix*, Fig. S7 and Movies S8 and S9, but this does not impair our conclusions about the effect of metachrony on fluid flow generation by MAC.

Discussion

In this paper, we have demonstrated a method to generate metachronal motion of MAC that exhibits a notable advantage in terms of facile miniaturization, a capability not attainable through previously reported methods. The proposed method involves the integration of a rod-shaped paramagnetic substructure beneath the MAC, which is magnetized by an applied external rotating magnetic field, generating a time-dependent local magnetic field at the location of the MAC. When well designed, neighboring cilia will experience a different magnetic field at any instant and metachronal motion will be realized even if the external magnetic field is uniform and the MAC are identical. The wavelength of the metachronal motion generated by this method is determined by the geometry and dimension of the paramagnetic substructure. Furthermore, our method facilitates the realization of diverse metachronal wave traveling directions through the manipulation of the relative position between the MAC and the underlying magnetic substructure, so that, uniquely, both symplectic and antiplectic metachrony can be realized.

The motion of each individual magnetic artificial cilium is determined by the balance between magnetic and elastic torques over time, and hence by the cilia bending stiffness which results from the cilia shape and size (18). In this study, we have chosen for the regular cylindrical shape (with an aspect ratio of six), primarily to be consistent with most MAC reported previously in the literature. However, cilia in nature often have a larger aspect ratio and are often tapered, and as a result of pathological conditions, aberrant shapes may occur such as long, whip-like cilia and bulbous tips; this influences the cilia stiffness and thus their motion (38). The femtosecond laser machining process we used to fabricate the smaller cilia enables us to realize such complex shapes. We will address these aspects in our future work and investigate their potential impact on the performance of our artificial magnetically actuated cilia system.

We conducted a detailed investigation into the fluid flow generated by the two metachronal motions under both high and low Reynolds number conditions. We showed that inertia dominates the flow generation at high Reynolds numbers (in water), whereas this does not play a role at low Reynolds numbers (in glycerol); metachrony still has a substantial influence on the generated fluid flow at high Reynolds numbers, and the effect depends on the metachronal wave propagation direction. For low Reynolds number conditions, we showed that antiplectic metachronal motion enhances the flow velocity caused by the asymmetric motion of the MAC alone, whereas symplectic metachronal motion decreases it; this conclusion corresponds well with the previous numerical research. In this study, in contrast to earlier reports, two metachronal motions (symplectic versus antiplectic) have been experimentally realized for identical MAC actuated by a uniform external magnetic field. Our method breaks the size limitation of metachronal motion, which is a vital step toward integrating metachronal MAC in small-scale microfluidic chips. Next to this practical application, in the future, our method may also be used to mimic the metachronal motion of biological cilia at real-life scales, to study and understand the mechanisms of mucus transportation by cilia in the airways, or flow generation in other organs.

Materials and Methods

Fabrication of MAC. We fabricated two different sizes of MAC in this research: one with a diameter of 50 μm and a height of 300 μm, and the other is 2 times smaller, with a diameter of 25 μm and a height of 150 μm. The molds for the differently sized MAC were made by two different methods as shown in Fig. 1*A*: The mold for large MAC is made by photolithography, while the mold for the miniaturized MAC is made by femtosecond laser machining. The femtosecond laser–machined mold is salinized prior to using it. The following steps of MAC fabrication are identical for the two mold types: 1) Spray a layer of Ease Release 200 (Smooth-On, Japan) on the prepared molds and place them in vacuum for 10 min to make sure that the sprayed layer is uniformly distributed over the mold surface. 2) A uniform magnetic precursor of Ecoflex 00-30 (Smooth-On, Japan) and paramagnetic particles (CIP, 99.5%, Sigma-Aldrich) is casted on the mold, followed by degassing in vacuum. The weight ratio of Ecoflex and CIP was 1:1; the weight ratio of Part A and Part B of Ecoflex 00-30 was 1:1. The specifics of the preparation procedure of the magnetic mixture are described in *SI Appendix*. 3) Wipe off the extra magnetic mixture on top of the mold with clean tissue. 4) Pour pure polydimethylsiloxane (PDMS, Sylgard 184, Dow Corning) with weight ratio of base and curing agent of 10:1 onto the mold and degas in vacuum in a desiccator for around 30 min. Note: As the Ecoflex is easily solidified at room temperature, we kept the vacuum desiccator at a low temperature by applying ice bags underneath the molds. To distribute the PDMS layer evenly over the surface, we use spin coating at a speed of 1,000 rpm for 50 s, resulting in a PDMS layer with a thickness of 100 μm. 5) Put a permanent magnet under the mold to align the magnetic particles within the microholes along the cilia length and leave the samples in an oven at 80° for 3 h to solidified. 6) Peel off the MAC off the mold under a stereo microscope. Note: we apply some isopropanol between the PDMS layer and the mold surface to decrease the adhesion, which makes the demolding process more smoothly. The final demolded large and small MAC are shown in Fig. 1 *B*, *ii* and *iii*, respectively.

Fabrication of Magnetic Substructure. The magnetic substructure was made by a PMMA mold as shown in Fig. 1*C*. The steps are similar to the fabrication procedure of MAC: 1) Make a cylindrical shape in a PMMA plate by laser cutting, with

a diameter of 4.5 mm and a depth of 6 mm. 2) Spray a layer of Ease Release 200 on the mold, which makes it easier to demold the structures later; subsequently placing the mold in vacuum is not necessary because of the relatively large size of the structure. 3) Fill the mold with a magnetic precursor mixture of PDMS and CIP with a weight ratio of 1:3. The weight ratio of PDMS base to curing agent is 10:1. The specific procedure of making the magnetic mixture is described in *SI Appendix*. 4) Remove the extra magnetic mixture outside the cylinder structure, on top of the PMMA mold, by a clean tissue. 5) Pour a layer of pure PDMS on top of the structure followed by degassing. 6) Peel off the magnetic substructure gently. 7) Laser-cut a rectangular shape in another PMMA plate. The width of the rectangle is 4.5 mm, equal to the diameter of the cylindrical structure to make sure that the distance between the top of the magnetic structure and the PDMS flat surface is as small as possible. 8) Put the demolded magnetic structure in the rectangular mold and fill the remaining space with pure PDMS, followed by degassing in vacuum. 9) Leave the samples in an oven at 80° for 2 h. 10) Peel off the magnetic substructure and flat PDMS surface. The schematic and real image of the magnetic substructure are shown in Fig. 1 *B*, *i* and *iv*, respectively.

Actuation Setup. A home-built rotating uniform magnetic field was used to actuate the MAC, schematically shown in Fig. 1 *D*, *i*. The actuation setup consists of two permanent magnets (50 × 50 × 12.5 mm^3, remnant flux density of 1.2 T, Q-50- 50-12.5-N, Supermagnete, Germany) with opposite poles at 50 mm distance supported by a PMMA frame. The magnetic field generated by the parallel magnets is about 150 mT in the center. The magnets are driven by an electric motor, which can be controlled by an in-house program through commercial software (Escon Studio). A PMMA holder is made to support the samples in the center of the uniform magnetic field; its position can be adjusted by an external XYZ stage.

Characterization of MAC Motion. To characterize the motion of the MAC, we made a sample holder by 3D printing (Form 3 SLA printer, Formlabs) as shown in Fig. 1 *D*, *ii*. The integrated MAC and magnetic substructure are put at the right position in the front of the channel, which has a length of 4.5 mm, a width of 6 mm, and a height of 4.5 mm. To observe the MAC motion in water and glycerol clearly, a transparent glass substrate was glued in front of the 3D printed channel. The width of the channel is 6 mm. A high-speed camera (Phantom, USA) mounted on a stereo microscope (Olympus, SZ61) was used to capture the MAC motion in a side view both in water and glycerol. The recording frequency was 1,000 times the beating frequency of the MAC. We used ImageJ to analyze the tip trajectories and to quantify the tip speed, swept area, and opening angle of the MAC motion.

Characterization of Flow Generation. We observed the flow from the side opposite to the MAC array as shown in Fig. 1 *D*, *iii* and *SI Appendix*, Fig. S1. A PDMS holder allowing for proper positioning of the magnetic substructure was made by casting PDMS into a 3D printed mold. The dimensions of the container for the magnetic substructure are 4.5 mm in length, 6 mm in width, and 4.5 mm in height. The flow channel was made also by the same method, with a width of 3 mm. We made an inlet and an outlet on top using a 1.2-mm puncher. To observe the flow clearly, we bonded a transparent glass substrate in front of the PDMS channel by plasma treatment. Then, we integrated the flow channel with the PDMS holder, again, by plasma treatment. The liquids used in the research were deionized water and pure glycerol, respectively. To visualize the flow, we added red-colored polystyrene tracer particles with a diameter of 10 μm (PS-Red-10.5, microParticles GmbH, Germany). We used a CMOS camera (DFK 33UX252) connected to a stereo microscope to capture the flow speed at 1 frame per second (fps) for both liquids. The optical system was focused at the center of the channel, as shown by the red dashed line in Fig. 1 *D*, *iii*. The videos were analyzed by ImageJ to quantify the flow speed. To get the flow speed at each frequency, at least three independent experiments were done, and ten independent measurements were done for each experiment, from which we obtained the average flow speed and SD.

Data, Materials, and Software Availability. All study data are included in the article and/or supporting information.

ACKNOWLEDGMENTS. This research was funded by the European Research Council Advanced Grant Bio-Plan project under grant agreement no. 833214. Z.C. is financially supported by the China Scholarship Council under grant no. 201706400061. S.Z. is financially supported by the Alexander von Humboldt Foundation.

1. B. Chakrabarti, S. Fürthauer, M. J. Shelley, A multiscale biophysical model gives quantized metachronal waves in a lattice of beating cilia. *Proc. Natl. Acad. Sci. U.S.A.* **119**, 1–9 (2022).
2. R. Zhang, J. den Toonder, P. R. Onck, Metachronal patterns by magnetically-programmable artificial cilia surfaces for low Reynolds number fluid transport and mixing. *Soft Matter* **18**, 3902–3909 (2022).
3. S. Zhang, Z. Cui, Y. Wang, J. M. J. Den Toonder, Metachronal actuation of microscopic magnetic artificial cilia generates strong microfluidic pumping. *Lab Chip* **20**, 3569–3581 (2020).
4. B. Gorissen, M. De Volder, D. Reynaerts, Pneumatically-actuated artificial cilia array for biomimetic fluid propulsion. *Lab Chip* **15**, 4348–4355 (2015).
5. S. N. Khaderi *et al.*, Magnetically-actuated artificial cilia for microfluidic propulsion. *Lab Chip* **11**, 2002–2010 (2011).
6. J. Elgeti, G. Gompper, Emergence of metachronal waves in cilia arrays. *Proc. Natl. Acad. Sci. U.S.A.* **110**, 4470–4475 (2013).
7. E. Milana, B. Gorissen, S. Peerlinck, M. De Volder, D. Reynaerts, Artificial soft cilia with asymmetric beating patterns for biomimetic low-reynolds-number fluid propulsion. *Adv. Funct. Mater.* **29**, 1–8 (2019).
8. S. Hanasoge, P. J. Hesketh, A. Alexeev, Metachronal actuation of microscale magnetic artificial cilia. *ACS Appl. Mater. Interfaces* **12**, 46963–46971 (2020).
9. X. Dong *et al.*, Bioinspired cilia arrays with programmable nonreciprocal motion and metachronal coordination. *Sci. Adv.* **6**, 1–14 (2020).
10. S. M. Vanaki *et al.*, Muco-ciliary clearance: A review of modelling techniques. *J. Biomech.* **99**, 109578 (2020).
11. X. M. Bustamante-Marin, L. E. Ostrowski, Cilia and mucociliary clearance. *Cold Spring Harb. Perspect. Biol.* **9**, 1–18 (2017).
12. H. Gu *et al.*, Magnetic cilia carpets with programmable metachronal waves. *Nat. Commun.* **11**, 1–10 (2020).
13. S. Gueron, K. Levit-Gurevich, Energetic considerations of ciliary beating and the advantage of metachronal coordination. *Proc. Natl. Acad. Sci. U.S.A.* **96**, 12240–12245 (1999).
14. S. Chateau, J. Favier, U. D'Ortona, S. Poncet, Transport efficiency of metachronal waves in 3D cilium arrays immersed in a two-phase flow. *J. Fluid Mech.* **824**, 931–961 (2017).
15. E. Milana *et al.*, Metachronal patterns in artificial cilia for low Reynolds number fluid propulsion. *Sci. Adv.* **6**, 1–8 (2020).
16. S. Zhang, Z. Cui, Y. Wang, J. Den Toonder, Metachronal **μ**-cilia for on-chip integrated pumps and climbing robots. *ACS Appl. Mater. Interfaces* **13**, 20845–20857 (2021).
17. J. R. Blake, M. A. Sleigh, Mechanics of ciliary locomotion. *Biol. Rev. Camb. Philos. Soc.* **49**, 85–125 (1974).
18. T. ul Islam, *et al.*, Microscopic artificial cilia–A review. *Lab Chip* **22**, 1650–1679 (2022).
19. Q. Zheng, Z. L. Wu, Light-steered locomotion of muscle-like hydrogel by self-coordinated shape change and friction modulation. *Nat. Commun.* **11**, 5166 (2020).
20. C. L. Van Oosten, C. W. M. Bastiaansen, D. J. Broer, Printed artificial cilia from liquid-crystal network actuators modularly driven by light. *Nat. Mater.* **8**, 677–682 (2009).
21. J. Den Toonder *et al.*, Artificial cilia for active micro-fluidic mixing. *Lab Chip* **8**, 533–541 (2008).
22. N. Osterman, A. Vilfan, Finding the ciliary beating pattern with optimal efficiency. *Proc. Natl. Acad. Sci. U.S.A.* **108**, 15727–15732 (2011).
23. S. N. Khaderi, J. M. J. den Toonder, P. R. Onck, Fluid flow due to collective non-reciprocal motion of symmetrically-beating artificial cilia. *Biomicrofluidics* **6**, 014016 (2012).
24. R. Zhang, J. den Toonder, P. R. Onck, Transport and mixing by metachronal waves in nonreciprocal soft robotic pneumatic artificial cilia at low Reynolds numbers. *Phys. Fluids* **33**, 092009 (2021).
25. F. Meng, R. R. Bennett, N. Uchida, R. Golestanian, Predicting the properties of metachronal waves from single-cilium characteristics. *Soft Condensed Matter* **1**, 1–5 (2020).
26. J. Hall, N. Clarke, The mechanics of cilium beating: Quantifying the relationship between metachronal wavelength and fluid flow rate. *J. Fluid Mech.* **891**, A20 (2020).
27. S. Gueron, K. Levit-Gurevich, N. Liron, J. J. Blum, Cilia internal mechanism and metachronal coordination as the result of hydrodynamical coupling. *Proc. Natl. Acad. Sci. U.S.A.* **94**, 6001–6006 (1997).
28. S. N. Khaderi, J. M. J. Den Toonder, P. R. Onck, Microfluidic propulsion by the metachronal beating of magnetic artificial cilia: A numerical analysis. *J. Fluid Mech.* **688**, 44–65 (2011).
29. S. Hanasoge, P. J. Hesketh, A. Alexeev, Microfluidic pumping using artificial magnetic cilia. *Microsystems Nanoeng.* **4**, 11 (2018).
30. T. Niedermayer, B. Eckhardt, P. Lenz, Synchronization, phase locking, and metachronal wave formation in ciliary chains. *Chaos* **18**, 037128 (2008).
31. S. Hanasoge, P. J. Hesketh, A. Alexeev, Metachronal motion of artificial magnetic cilia. *Soft Matter* **14**, 3689–3693 (2018).
32. R. Marume, F. Tsumori, K. Kudo, T. Osada, K. Shinagawa, Development of magnetic-field-driven artificial cilium array with magnetic orientation in each cilium. *Jpn. J. Appl. Phys.* **56**, 06GN15 (2017).
33. F. Tsumori *et al.*, Metachronal wave of artificial cilia array actuated by applied magnetic field. *Jpn. J. Appl. Phys.* **55**, 06GP19 (2016).
34. L. Pedersoli *et al.*, Engineered modular microphysiological models of the human airway clearance phenomena. *Biotechnol. Bioeng.* **118**, 3898–3913 (2021).
35. H. Shinoda, F. Tsumori, "Development of micro pump using magnetic artificial cilia with metachronal wave" in *Proc. IEEE Int. Conf. Micro Electro Mech. Syst. 2020-Janua*, (IEEE, 2020), pp. 497–500.
36. Z. Cui *et al.*, Self-cleaning surfaces realized by biologically sized magnetic artificial cilia. *Adv. Mater. Interfaces* **9**, 2102016 (2021).
37. T. Ul Islam, Y. Bellouard, J. M. J. Den Toonder, Highly motile nanoscale magnetic artificial cilia. *Proc. Natl. Acad. Sci. U.S.A.* **118**, 35 (2021).
38. A. S. Shah *et al.*, Loss of Bardet-Biedl syndrome proteins alters the morphology and function of motile cilia in airway epithelia. *Proc. Natl. Acad. Sci. U.S.A.* **105**, 3380–3385 (2008).